Catal Lett (2008) 120:244–251
DOI 10.1007/s10562-007-9276-5

Fe-ZSM-5 Catalysts: Preparation in Organic Media, Fe-particle Morphology and NO_x Reduction Activity

**Enrique Lima · Ariel Guzmán-Vargas ·
Juan Méndez-Vivar · Heriberto Pfeiffer ·
Jacques Fraissard**

Received: 25 July 2007 / Accepted: 10 September 2007 / Published online: 29 September 2007

Abstract Fe-ZSM5 catalysts were prepared at room temperature. Iron was incorporated into H-ZSM5 in organic media (toluene) using iron acetyl acetonate. In order to elucidate the catalytic performance of this Fe-ZSM5, reference catalysts were prepared by chemical vapour deposition (CVD) and impregnation in aqueous media (IMW). The various catalysts were characterized structurally and morphologically. Materials prepared in organic media and CVD showed fibrous iron particles, with radius between 10 and 40 Å, highly dispersed on the external zeolite surface. Fractal dimension values suggest that iron particles grow dendritically when iron is incorporated into zeolite by impregnation in organic media. Nuclear magnetic resonance of ^{129}Xe adsorbed on catalysts shows that dendrites can penetrate into the zeolite channels. The dispersion of the iron species on the external surface of the zeolite and the presence of iron inside the channels explain the good catalytic performance in the Selective Catalytic Reduction (SCR) of NO. Ammonia and *n*-decane were employed as reducing agents. The highest NO to N_2 conversion ($\approx$100% at 430 °C) was obtained when ammonia was used. In contrast, n-decane is unable to reach Fe species in channels, and the inner active surface is thus lost.

Keywords NO_x reduction · Zeolite · Xenon NMR

1 Introduction

HZSM5 zeolite has been applied as a catalyst in many processes and reactions, such as the production of synthetic gasoline, isomerization, cracking and reforming [1, 2]. Additionally, in recent years, modified zeolites have attracted attention for their performance in many other applications. For instance, zeolites containing transition metal ions show high activities in the Selective Catalytic Reduction (SCR) of nitrogen oxides, NO_x, which must be eliminated since they contribute to the ozone clouds and acid rain formation [3, 4].

Fe-ZSM5 catalysts have been extensively used for this elimination [5–8]. The studies have focused mainly on the nature of the iron species [9–12]. It has been stated that the formation of iron species depends strongly on the preparation method. Several iron complexes have been reported as active species in the SCR NO_x reaction. Preparation under water-free conditions, as in chemical vapour deposition (CVD), has been studied by many groups. Sachtler et al. [11] and Battiston et al. [13] have reported a binuclear active species $[HO\text{–}Fe\text{–}O\text{–}Fe\text{–}OH]^{2+}$ as the compensating charge in the zeolite framework. On the contrary, Marturano et al. [14, 15] claim that the active species is $[HO\text{–}Fe(\mu\text{-}OH)_2\text{–}Fe\text{–}OH]^{2+}$. Recently, Krisnha

E. Lima (✉) · J. Méndez-Vivar
Universidad Autónoma Metropolitana, Iztapalapa,
Av. San Rafael Atlixco No. 186 Col. Vicentina,
09340 México, DF, Mexico
e-mail: lima@xanum.uam.mx

A. Guzmán-Vargas
Instituto Politécnico Nacional – ESIQIE, Av. IPN UPALM Edif.
7 Planta Baja, México 07738 México, DF, Mexico

H. Pfeiffer
Instituto de Investigaciones en Materiales, Universidad Nacional
Autónoma de México, Ciudad Universitaria, 04510 México, DF,
Mexico

J. Fraissard
Laboratoire de Physique Quantique, Université Pierre et Marie
Curie and ESPCI, 10 Rue Vauquelin, 75231 Paris cedex 05,
France

et al. [16] in a CVD preparation, reported a hydroxide iron species, [$Fe(OH)_2$]. Preparation in the presence of water promotes the formation of different iron species. The model suggested by Lobree et al. [12] consists of FeO_x particles, while Joyner et al. [9] reported iron-oxo nanoclusters like Fe_4O_4. Schwidder et al. [17] showed that the iron species formed is directly correlated with the iron content. Thus, at low content the iron is present as mononuclear sites (Fe^{2+} cations). On the contrary, at high iron loading there is evidence that oligomeric entities (Fe_xO_y) and mononuclear species coexist.

All these species have shown activity in the SCR of NO with hydrocarbons and ammonia. Nevertheless, according to the literature, the most active iron species are formed under water-free conditions. Although much work has been reported on the role of the iron species in catalysis, only a few contributions have paid attention to morphological aspects [18].

In this article we report the preparation of Fe-ZSM5 catalysts by impregnation in organic media with a particular focus to the morphology of the iron species. The characteristics and catalytic performance of Fe-ZSM5 prepared in organic media are compared with those of Fe-ZSM5 prepared in aqueous media and CVD.

2 Experimental

2.1 Materials Preparation

The parent zeolite was NH_4-ZSM5 (Zeolyst CBV3024E, Si/Al = 15, S_{BET} = 400 m^2 g^{-1}). Protonated zeolite, H-ZSM5, was obtained by calcination of NH_4-ZSM5 in air at 550 °C. Iron sources, $Fe(acac)_3$, $FeCl_3$ (Aldrich) and $Fe(NO_3)_3 \cdot 9H_2O$ (Fluka) were used without further purification. Iron incorporation into H-ZSM5 was performed in three different ways: impregnation in aqueous media (IMW), chemical vapour deposition (CVD), and impregnation in organic media (IMO). Depending on the preparation method the samples were labelled Fe(x)-ZSM5-IMW, CVD and IMO with x = molar Fe/Al ratio.

Impregnation in aqueous media: *Fe(0.65)-ZSM5-IMW, Fe(0.87)-ZSM5-IMW.*

An amount of $Fe(NO_3)_3 \cdot 9H_2O$ solution containing the quantity of iron required to reach the nominal Fe content in the catalyst was put into contact with NH_4-ZSM5 at 25 °C. The solid was then dried at 80 °C and calcined in air at 550 °C.

$FeCl_3$ sublimation: *Fe(0.5)-ZSM5-CVD, Fe(0.83)-ZSM5-CVD.*

These two catalysts were prepared by subliming $FeCl_3$ according to the protocol reported by Chen and Sachtler [19]. Prior to sublimation phase, 2 g of HZSM-5 were calcined at 450 °C under dry air while $FeCl_3$ was dried at 120 °C. H-ZSM-5 and $FeCl_3$ were then heated slowly (ramp 0.5 °C min^{-1}) under argon atmosphere (10 mL min^{-1}) from 100 to 316 °C (sublimation temperature of $FeCl_3$). The temperature was maintained at 316 °C in Ar flow for 3 h and cooled to room temperature. Then the solids were washed tree times with deionized water and then dried at 80 °C overnight and lastly calcined at 550 °C (ramp 5 °C min^{-1}) under air flow (40 mL min^{-1}) during 3 h.

Preparation in organic media: *Fe(0.95)-ZSM5-IMO, Fe(0.21)-ZSM5-IMO.*

H-ZSM5 was put into contact with a solution of $Fe(acac)_3$ in toluene for 24 h at room temperature with vigorous stirring. The solvent was then evaporated and the solid calcined in air at 550 °C.

2.2 Characterization

The materials were characterized by transmission electronic microscopy (TEM), X-ray diffraction (XRD), small-angle X-ray scattering (SAXS), xenon adsorption and ^{129}Xe, ^{27}Al, ^{29}Si nuclear magnetic resonance (NMR) spectroscopies.

TEM analysis was performed in a JEOL JEM-1200EX transmission electron microscope to obtain bright-field images at 200 kV. The powder samples were prepared using standard methods.

The XRD powder patterns were obtained with a Siemens D-5000 diffractometer coupled to a copper X-ray anode. Kα radiation was selectively monochromated using a Ni filter. Conventional identification of crystalline compounds was performed by comparing the diffractograms with JCPDS (Joint Committee on Powder Diffraction Standards) files.

Small-angle X-ray scattering experiments were performed with a Kratky camera coupled to a copper anode tube. The distance between the sample and the linear proportional counter was 25 cm; a Ni filter selected the copper K_α radiation. In order to avoid any interference or absorption of the sample holder, the powdered sample was packed in the window of an aluminium sample holder.

SAXS data were processed with the ITP program where the angular parameter (h) is defined as $h = 2\pi \sin\theta/\lambda$; θ and λ are the X-ray scattering angle and the wavelength, respectively. The shape of the scattering objects was estimated from the Kratky plot, i.e., h^2 I(h) against h [20–24]. The shape is determined from that of the Kratky curve; for instance, if the curve presents a peak the particles are globular.

From the slope of the Log I(h) versus Log(h) curve the fractal dimension of the scattering objects was calculated. The h interval was $0.07 < h < 0.18$ Å^{-1}.

One-pulse solid-state ^{27}Al MAS NMR spectra were obtained at a frequency of 78.15 MHz on a Bruker ASX 300 spectrometer using a 4 mm MAS probe with a spinning rate of 10 kHz. The calibrated $\pi/2$ pulse was 2 μs and the repetition time 0.5 s. Chemical shifts were referenced to 1 N $AlCl_3$ solution. ^{29}Si MAS NMR spectra were recorded at 59.591 MHz. Direct pulsed NMR excitation was used throughout, employing 90° observing pulses (3 μs) with a pulse repetition time of 8 s. Powdered samples were packed in zirconia rotors. Spinning rate was 5 kHz. Chemical shifts were referenced to TMS.

Xenon gas containing 99.99% of 129 isotope was used for the ^{129}Xe NMR measurements. For these experiments, the sample powder was placed in an NMR tube, then xenon was adsorbed at room temperature at different pressures. Prior to xenon loading, samples were dehydrated by gradual heating up to 673 K in vacuum (1.33×10^{-4} kPa). ^{129}Xe NMR spectra were recorded in a Bruker DMX-500 spectrometer operating at 138.34 MHz. Single excitation pulses were used and at least 1,000 scans were collected with a delay time of 2 s. The chemical shift was referenced to xenon gas extrapolated to zero pressure.

2.3 Catalytic Tests

The selective catalytic reduction (SCR) of NO was tested under continuous flow conditions using a tubular fixed-bed reactor operating at atmospheric pressure, placed in an electric furnace. The catalysis tests were carried out following a temperature-programmed surface reaction protocol (TPSR) from 200 °C up to 550 °C (heating rate, 10 °C min^{-1}). The tubular reactor was loaded with powder catalyst ($\sim$100 mg). Prior to reaction the solid was activated in situ at 550 °C in air (O_2/N_2: 20/80) for 2 h and then cooled to 200 °C. The reaction was carried out with two different reductants with typical exhaust gas composition: (1) n-decane: a mixture of NO/n-decane/O_2/He (0.1/0.03/9.0/90.87%) was fed into the reactor, giving a gas hourly space velocity (GHSV) of 35,000 h^{-1}. (2) NH_3: the feed composition was: NO/NH_3/O_2/He (0.2/0.2/3.0/96.4%) giving a GHSV of 332,000 h^{-1}. Note that GHSV are different because *n*-decane was used as a model molecule of diesel (diesel engines) and ammonia was employed for emissions from stationary sources. The output gas composition (NO, NH_3, N_2O, *n*-decane) was monitored continuously by sampling on-line using a quadruple mass spectrometer (Pfeiffer Omnistar) equipped with Channeltron and Faraday detectors (0–200 amu). The quantities of CO and CO_2 produced and n-decane eliminated during SCR with *n*-decane were determined with a Bruker Vectra 22 IR spectrometer equipped with a gas cell.

3 Results and Discussion

3.1 Characterization

Figure 1 displays the XRD patterns of Fe-containing zeolites. All diffractograms correspond to ZSM5 zeolite. No iron compounds were identified in the samples prepared by CVD or by impregnation in organic media. In contrast, in the sample Fe(0.87)-ZSM5-IMW, prepared in aqueous media, haematite was detected.

^{27}Al MAS NMR spectra show that the aluminium remains predominantly in tetrahedral coordination (signal close to 50 ppm), independently of the method used for iron incorporation (Fig. 2). A small peak near 0 ppm, due to six-fold coordinated aluminium, was detected. This signal is not a consequence of the iron loading, because it

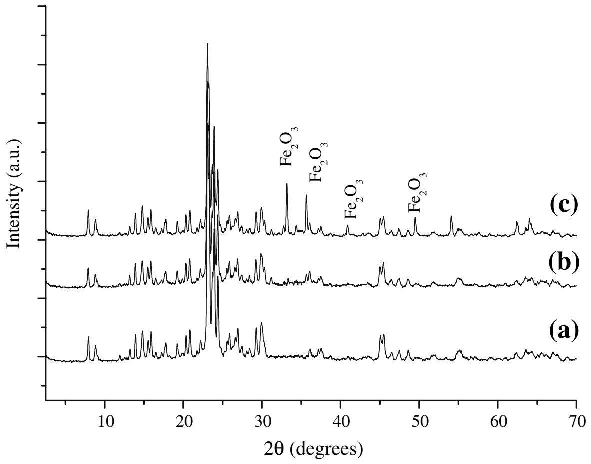

Fig. 1 X-Ray diffraction patterns of Fe(0.5)-ZSM5-CVD (a), Fe(0.96)-ZSM5-IMO (b) and Fe(0.87)-ZSM5-IMW (c). Peaks labelled Fe_2O_3 correspond to haematite phase

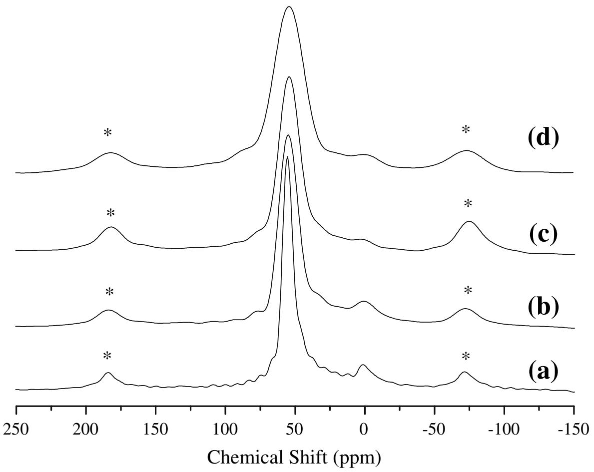

Fig. 2 ^{27}Al MAS NMR spectra of H-ZSM5 (a), Fe(0.87)-ZSM5-IMW (b), Fe(0.5)-ZSM5-CVD (c) and Fe(0.96)-ZSM5-IMO (d). * indicates spinning side bands

was also present in the starting zeolite. The only significant effect on the ^{27}Al NMR signals of iron loading is peak broadening. The broadest peak was observed in the spectra of samples prepared in organic media, Table 1. This suggests the presence of iron inside channels.

The ^{29}Si MAS NMR spectra displayed in Fig. 3 reveal that the zeolite framework does not change as a consequence of iron incorporation, independently of the method used. Spectra are dominated by signals between –100 and –118 ppm. As an example, the decomposition of the spectrum corresponding to Fe(0.96)-ZSM5-IMO is shown, Fig. 3(d). The zeolite framework consists mainly of Si(0Al) and Si(1Al) units, with peaks close to –117 and –113 ppm, respectively. Peaks at lower field, –109 and –105 ppm, are assigned to Si(2Al) and Si(3Al) units, and they are present in smaller quantities [25, 26]. None of the methods used to incorporate iron into zeolite produces significant changes in the distribution of Si(nAl) units. Thus the introduction of iron does not lead to oxo-iron species bonded directly to Si–O–Si. As observed in the case of ^{27}Al NMR spectra, in the ^{29}Si NMR peaks are slightly broadened by iron incorporation.

Figure 4 presents the xenon isotherms of the various samples. The uptake tends toward saturation at pressures as high as 135–140 kPa. All the samples containing iron have lower xenon adsorption capacities than the iron-free one. This was expected because of the decrease in the free space in the zeolite channels. However, this result itself cannot discriminate between two situations, where the channels are partially or completely filled with small iron particles or where the entry of the channels is blocked by bigger particles. The isotherms are more illustrative if they are discussed together with the ^{129}Xe NMR results.

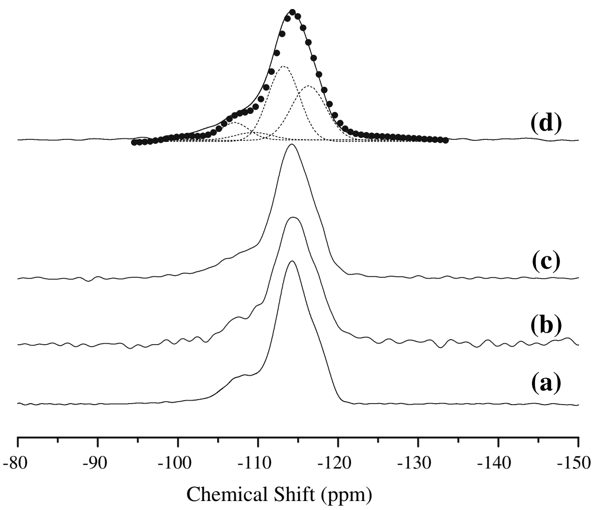

Fig. 3 ^{29}Si MAS NMR spectra of H-ZSM5 (a), Fe(0.87)-ZSM5-IMW (b), Fe(0.5)-ZSM5-CVD (c), and Fe(0.96)-ZSM5-IMO (d). Deconvolution of spectrum in (d): dashed lines correspond to individual contributions and their sum is the dotted line; solid line represents the experimental spectrum

The ^{129}Xe NMR spectra of xenon adsorbed at 6.6 kPa are exhibited in Fig. 5. They all consist of a single signal; the peaks are broader in the iron-containing zeolites than in free iron, especially for CVD and IMO, as reported in Table 1. Figure 6 presents the increase in the chemical

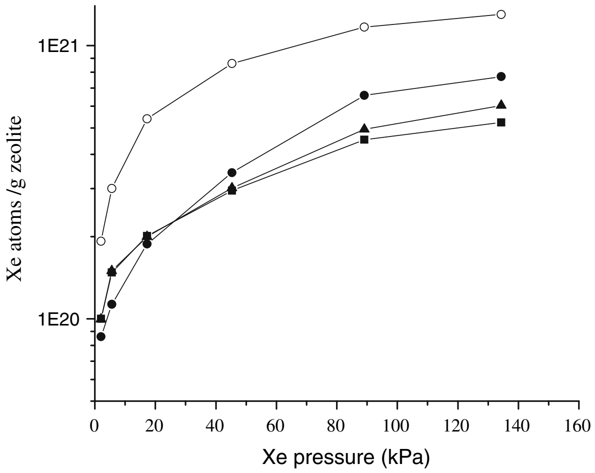

Fig. 4 Xenon uptake as a function of pressure: (○) H-ZSM5, (●) Fe(0.87)-ZSM5-IMW, (▲) Fe(0.5)-ZSM5-CVD, and (■) Fe(0.21)-ZSM5-IMO

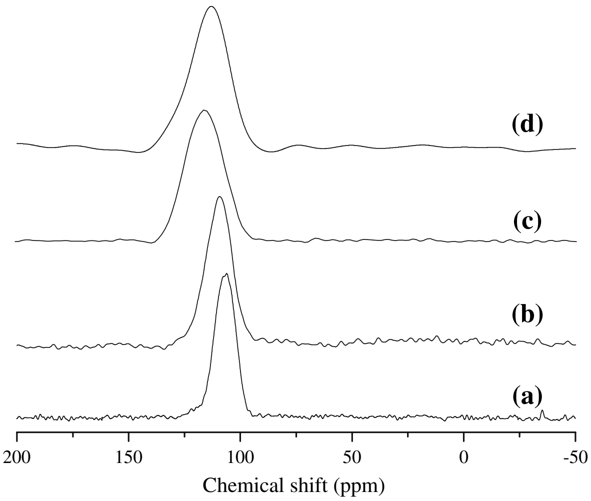

Fig. 5 ^{129}Xe NMR spectra of xenon adsorbed (6.6 kPa) on H-ZSM5 (a), Fe(0.87)-ZSM5-IMW (b), Fe(0.5)-ZSM5-CVD (c), and Fe(0.21)-ZSM5-IMO (d)

Table 1 Line width of ^{27}Al and ^{129}Xe resonances of various samples

Sample	Line width (Hz)	
	^{27}Al resonance	^{129}Xe resonance
H-ZSM5	718	841
Fe(0.87)-ZSM5-IMW	1,446	922
Fe(0.5)-ZSM5-CVD	1,451	1,576
Fe(0.96)-ZSM5-IMO	2,035	1,587

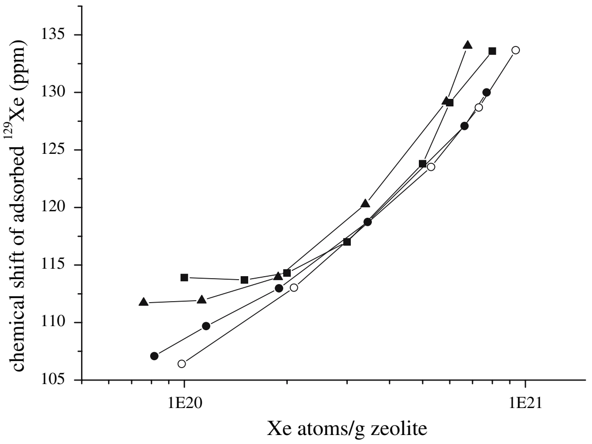

Fig. 6 ^{129}Xe chemical shift as a function of concentration of xenon in (○) H-ZSM5, (•) Fe(0.87)-ZSM5-IMW, (▲) Fe(0.5)-ZSM5-CVD, and (■) Fe(0.21)-ZSM5-IMO

shift, δ(Xe), with xenon concentration,. The curve for HZSM5 is consistent with the literature data. On the contrary, the iron-loaded samples show higher chemical shifts at low Xe concentration; such behaviour is particularly evident in the samples prepared by CVD and in organic media, while those prepared in aqueous media behave more like the iron-free zeolite. These NMR results, the peak broadening and greater chemical shift at low Xe concentration prove that xenon interacts with Fe sites, and therefore confirms the presence of iron particles inside the zeolite channels.

According to references [27, 28], the chemical shift of xenon in our samples can be expressed as follows:

$$\delta = \delta_0 + \delta_{\mathrm{Xe-W}} + \delta_{\mathrm{Xe-Fe}} + \delta_{\mathrm{Xe-Xe}}$$

δ_0 is the reference (adsorbed Xe extrapolated to zero pressure); $\delta_{\mathrm{Xe-W}}$ corresponds to the interactions between xenon atoms and zeolite pores; $\delta_{\mathrm{Xe-Fe}}$ is the part arising from the interaction of xenon atoms with iron particles located inside the pores, independently of the nature of this factor (electrostatic and/or magnetic); $\delta_{\mathrm{Xe-Xe}}$ is caused by xenon-xenon collisions. The influence of the variation of OH concentration with iron incorporation is negligible. The particles inside the pores cause an increase in the chemical shift at low xenon concentration because they are adsorption sites stronger than the pore walls. In contrast, at high xenon concentration δ increases also with this latter because Xe–Xe interactions become important. In the intermediate range of Xe concentration the shape of the curve depends on the influence of the particles. If this is low, the variation of δ against Xe concentration is monotonic and coincides quickly with the curve of H-ZSM5. On the contrary, if it is high δ starts to diminish with Xe concentration increase as a consequence of fast exchange with the atoms adsorbed on the other sites; then δ increases as Xe–Xe interactions become more important. Thus, the values of δ for Fe-containing samples differ from those for H-ZSM5 as a function of decreasing free space, which is a consequence of the presence of particles either inside the pores or blocking the entries to these pores.

The curve for sample IMW presents a slight increase in δ at low xenon concentration, then becomes similar to the curve of H-ZSM5. This result suggests the presence of a very small number of Fe particles inside the pores. In the case of samples CVD and IMO, the higher values of δ at low xenon loading reveal that there are in the pores either numerous iron-particles or more or less charged particles. The increase in δ at high xenon loading shows that the free volume is reduced, which suggests that the first of the two explanations is the more probable; the xenon isotherms further support this interpretation.

Figure 7 exhibits the Kratky plots of the three samples. Such profiles suggest that impregnation in aqueous media promotes the formation of iron particles with a spherical shape. In contrast, in the catalysts prepared by CVD and in organic media, the iron particles appear to be fibrous. From the SAXS data the fractal dimension of the iron particles in the various catalysts was determined, Table 2. Again, the solids prepared by aqueous impregnation present fractal dimensions different from those found for catalysts prepared by the other two methods. The catalysts obtained by IMW, CVD and IMO have fractal dimensions close to 2.9, 2.1, and 2.0, respectively. It is worth mentioning that fractal geometry may be regarded as a way of studying the effective geometry of the iron-containing particles. The values of fractal dimension are determined by the degree of surface roughness. The fractal dimension close to 2.9 indicates that iron particles in these catalysts are non-smoothed fractal mass but they have high irregularities or defects. In contrast, fractal dimensions close to 2 for the CVD and IMO series suggest a typical dendritic growth of these particles [29]. The geometry adopted by the Fe particles is, of course, a consequence of the geometry of the zeolite channels. The three-dimensional channel system of ZSM5 consists of 10-ring straight channels perpendicular to 10-ring sinusoidal channels, the section of pores being 5.3 × 5.6 Å and 5.1 × 5.5 Å, respectively. The channel geometry drives the arrangement of the host iron-containing particles and SAXS senses these particles as dendrites.

TEM results, Fig. 8, show the CVD and IMO samples to be very similar. Images show that there are nanoparticles on the surface of the zeolite. Part of the iron load is distributed on the external surface but a part is located inside the channels, as evidenced by the ^{129}Xe NMR of adsorbed xenon. It is worth mentioning that very small particles, prone to enter the channels, are not evident in the TEM images. At the highest magnification the electron beam caused destruction of the zeolite. Conversely, the values of

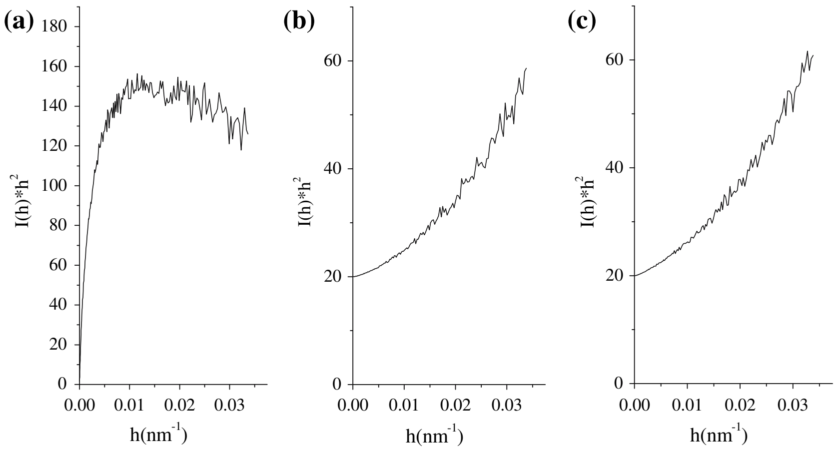

Fig. 7 Kratky plots of samples Fe(0.87)-ZSM5-IMW (a), Fe(0.5)-ZSM5-CVD (b), and Fe(0.96)-ZSM5-IMO (c)

Table 2 Fractal dimensions, as determined by SAXS data, of Fe-containing zeolites prepared by different methods

Sample	Fractal dimension
Fe(0.87)-ZSM5-IMW	2.9
Fe(0.5)-ZSM5-CVD	2.1
Fe(0.96)-ZSM5-IMO	2.0

TEM and the trends seem to disagree with the SAXS results, which report the formation of dendritic structures. This apparent contradiction may be explained by the principles of the techniques. SAXS curves are due to differences in electron densities of inhomogeneities on the materials, in the range of 10–500 Å. Therefore, the SAXS interpretation may refer to the internal structure of the iron particles, while TEM only shows the general shape. As a consequence, the fractal dimension determined has to be understood as a measure of roughness: impregnation in aqueous media promotes iron particles with a fractal mass close to 2.9. In contrast, the loading of iron by CVD or in organic media, promotes the growth of dendritic particles leading to a lower fractal dimension, i.e., the total mass of iron presents a greater dispersion.

3.2 Catalytic Activity

Figure 9 shows NO conversion in SCR using ammonia as reducing agent. At lower temperature, in general, the Fe(0.21)-ZSM5-IMO and Fe(0.96)-ZSM5-IMO solids show similar profiles. Nevertheless, a peculiar behaviour is observed between 200 and 250 °C with Fe(0.21)-ZSM5-IMO; this was reported in DeNO$_x$ reactions with ammonia on exchanged Fe-FER and Cu-FAU catalysts [30, 31]. It was suggested that the best conversion at lower temperature could be associated with ammonia radicals formed in situ which are more reactive toward NO than O_2, giving intermediates that finally yield N_2 and H_2O. When the temperature is increased a slight difference is noted between 350 and 500 °C; Fe(0.96)-ZSM5-IMO catalyst

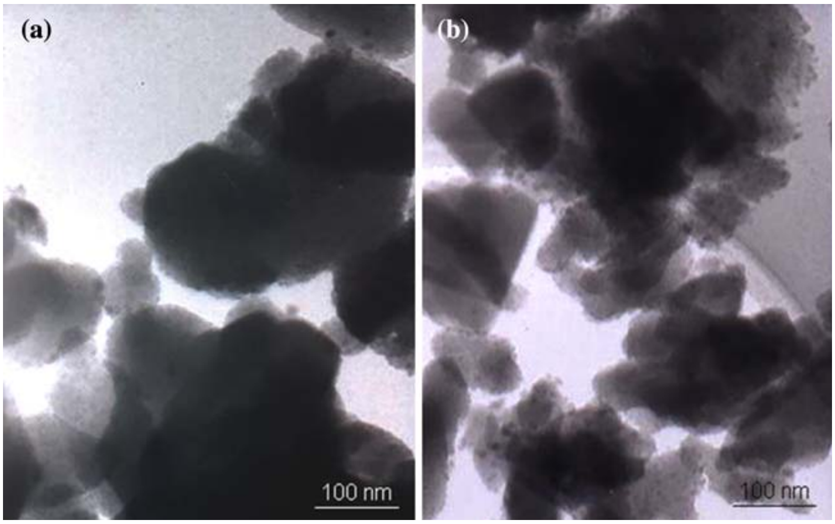

Fig. 8 Bright-field TEM images of iron-containing zeolites, Fe(0.5)-ZSM5-CVD (**a**) and Fe(0.96)-ZSM5-IMO (**b**)

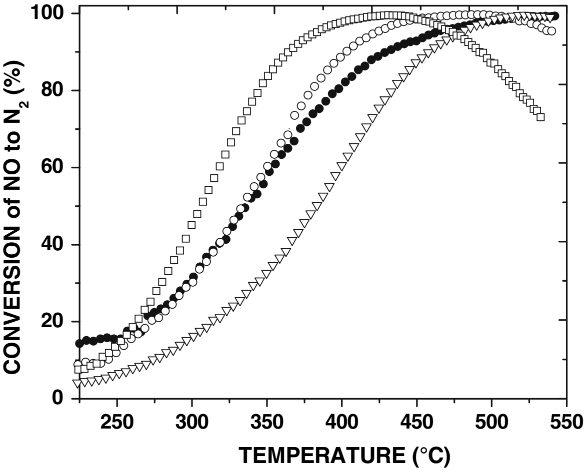

Fig. 9 Catalytic activity in NO reduction: SCR with NH_3 in TPSR mode over: (•) Fe(0.21)-ZSM5-IMO, (○) Fe(0.96)-ZSM5-IMO, (□) Fe(0.5)-ZSM5-CVD, (▽) Fe(0.87)-ZSM5-IMW. Conditions: NO/NH_3/O_2/He (0.2/0.2/3/96.6), GHSV = 332000 h^{-1}, heating rate = 7.5 K min^{-1}

reaches around 100% NO conversion at 450 °C, while Fe(0.21)-ZSM5-IMO shows a lower conversion (90%) at the same temperature. Clearly, Fe(0.5)-ZSM5-CVD is the best while Fe(0.87)-ZSM5-IMW is weakly active.

NO conversion diminishes at temperatures higher than 400 °C on Fe(0.5)-ZSM5-CVD catalysts; this feature is associated with ammonia oxidation at higher temperatures producing a deficiency of reductant and an excess of NO produced from the reaction between ammonia and oxygen ($2\ NH_3 + 2.5\ O_2 \rightarrow 2\ NO + 3\ H_2O$).

Figure 10 presents the catalytic activity in SCR of NO with n-decane. For all catalysts a volcano-like NO conversion profile is observed. NO conversion increases with reaction temperature and pass through maxima. Fe(0.21)-ZSM5-IMO, Fe(0.96)-ZSM5-IMO and Fe(0.5)-ZSM5-CVD materials reach maximal NO conversion (53%) at 400 °C. With IMW catalysts this maximum (45%) is obtained at higher temperature (435 °C).

Table 3 Conversion of NO with different catalysts, prepared by different methods

Catalyst	Conversion at 400 °C (%)		
	SCR with *n*-decane		SCR with NH_3
	NO conversion	*n*-Decane conversion	NO conversion
Fe(0.5)-ZSM5-CVD	53	100	98
Fe(0.87)-ZSM5-IMW	40	100	60
Fe(0.21)-ZSM5-IMO	51	100	81
Fe(0.96)-ZSM5-IMO	53	100	90

Regarding the hydrocarbon conversion, similar trends are observed for all catalysts, The maximum of conversion is obtained when the total oxidation of *n*-decane occurs.

Table 3 summarizes the activity of catalysts in NO reduction. Clearly, the materials prepared in water-free conditions, by the CVD and IMO methods, give the highest NO conversion, while the solid prepared by aqueous impregnation is the least active.

The Fe(0.5)-ZSM5-CVD, Fe(0.21)-ZSM5-IMO and Fe(0.96)-ZSM5-IMO solids contain small iron particles. SAXS along with ^{129}Xe NMR indicate that CVD and IMO catalysts host iron dendrites inside the zeolite channels. Thus, the reaction mixture can diffuse and react with the active iron sites producing a high NO conversion, i.e., the microporous surface is reached. In contrast, Fe(0.87)-ZSM5-IMW does not incorporate a large amount of iron into the channels, and catalysis is exclusively at the

Fig. 10 Catalytic activity in NO reduction: SCR with n-decane in TPSR mode over: Fe(0.21)-ZSM5-IMO (a), Fe(0.96)-ZSM5-IMO (b), Fe(0.5)-ZSM5-CVD (c), and Fe-(0.87)-ZSM5-IMW (d): (○) NO conversion to N_2, (•) n-decane conversion to CO + CO_2. Conditions: NO/n-decane/O_2/He (0.1/0.03/9/90.87), GHSV = 35000 h^{-1}

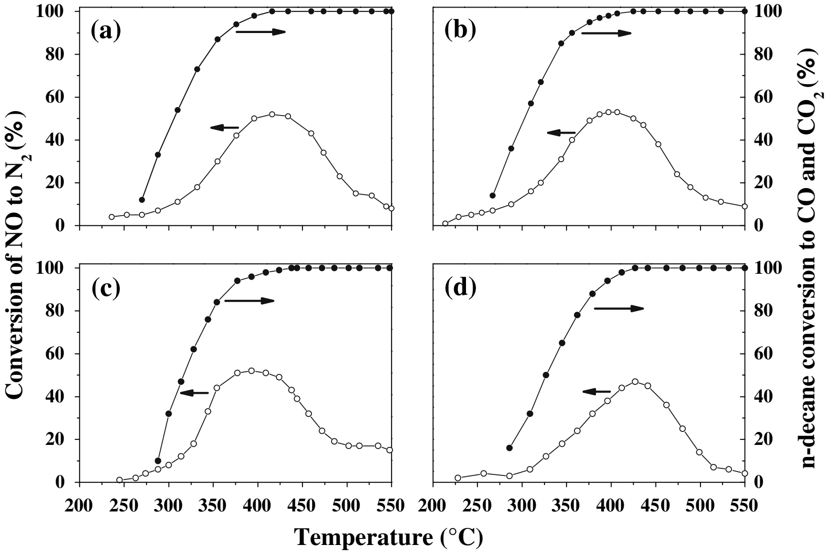

external surface where highly dense spherical particles are present, i.e., the inner surface is lost.

It should be mentioned that during SCR reactions with *n*-decane, the catalyst prepared by CVD shows 60% CO_2 yield (40% CO yield) at 400 °C (maximal NO conversion). The IMO and IMW solids show roughly the same behaviour (40% and 60% yield of CO_2 and CO, respectively, at the same temperature). Then, we can suggest that combustion products poison the actives sites giving a decrease in NO conversion. Nevertheless, it is important to mention that severe catalyst deactivation is mainly associated with the formation of nitrile species, which are easily polymerized [32, 33].

In summary, the catalysts exhibit higher catalytic activity when ammonia is used, instead of *n*-decane, as reductant. This result is explained by the inaccessibility of the zeolite channels to *n*-decane [34]. The reaction is exclusively catalysed by particles at the external surface. In this case the differences observed should be attributed to the nature of the species and their dispersion. As stated above, catalysts impregnated in aqueous media induce formation of large Fe_2O_3 particles whereas such large particles are not found in catalysts prepared by other means.

4 Conclusion

The preparation method is a determining factor affecting the location and morphology of iron particles in the zeolite support. Iron incorporation into the zeolite, by impregnation in aqueous media, promotes the formation of large spherical particles mainly on the external surface of the zeolite.

Instead, if a chemical vapour deposition or an impregnation organic media is used, well dispersed fibrilar iron nanoparticles are hosted at the external and inner surfaces of the zeolite. The iron particles in these catalysts can be associated to form dendrites entering even the void spaces of the zeolite.

Catalysts obtained by impregnation in organic media or chemical vapour deposition are more active in the SCR NO reaction because less dense iron particles are dispersed over the microporous surface of the zeolite.

Acknowledgments Thanks are due to M. A. Vera, V. Lara (UAMI) and C. Flores (IIM-UNAM) for technical help. AGV Thanks to LMCCCO- UMR 5618 CNRS-ENSCM-UM1, Montpellier, France. (Dr. Gérard Delahay). The support by CONACYT (grant No 49009) is gratefully acknowledged.

References

1. Csicsery CM (1984) Zeolites 4:202
2. Cappelazzo O, Cao G, Messina G, Morbidelli M (1991) Ind Eng Chem Res 30:2280
3. Pârvulescu VI, Grange P, Delmon B (1998) Catal Today 46:233
4. Traa Y, Burger B, Weitkamp J (1999) Microporous Mesoporous Mater 30:3
5. Hagen A, Roessner F, Weingart I, Spliethoff B (1995) Zeolites 15:270
6. Guzmán-Vargas A, Delahay G, Coq B, Lima E, Bosch P, Jumas JC (2005) Catal Today 107–108:94
7. Chen H-Y, Voskoboinikov T, Sachtler WMH (1999) Catal Today 54:483
8. Long RQ, Yang RT (1999) J Am Chem Soc 121:5595
9. Joyner RW, Stockenhuber M (1997) Catal Lett 45:15
10. Malki E-ME, Santen RAV, Sachtler WMH (1999) J Phys Chem B 103:4611
11. Chen HY, Voskoboinikov T, Sachtler WMH. (1998) J Catal 180:171
12. Lobree LJ, Hwang I-C, Reimer JA, Bell AT (1999) J Catal 186:242
13. Battiston AA, Bitter JH, Groot FMFD, Overweg AR, Stephan O, Bokhoven JAV, Kooyman PJ, Speck CVD, Vankó G, Koningsberger DC (2003) J Catal 213:251
14. Marturano P, Drozdová L, Pirngruber GD, Kogelbauer A, Prins R (2001) Phys Chem Chem Phys 3:5585
15. Marturano P, Drozdová L, Kogelbauer A, Prins R (2000) J Catal 192:236
16. Krishna K, Seijger GBF, Bleek CMVD, Makkee M, Mul G, Calis HPA (2003) Catal Lett 86:121
17. Schwidder M, Kumar MS, Klementiev K, Pohl MM, Brückner A, Grünert W (2005) J Catal 231:314
18. Pérez-Ramirez J, Mul G, Kapteijn F, Moulijn JA, Overweg AR, Doménech A, Ribera A, Arends IWCE (2002) J Catal 207:113
19. Chen HY, Sachtler WMH (1998) Catal Lett 50:125
20. Glatter O (1981) J Appl Cryst 14:101
21. Glatter O, Hainisch B (1984) J Appl Cryst 17:435
22. Glatter O (1988) J Appl Cryst 21:886
23. Glatter O (1991) Prog Colloid Polymer Sci 84:46
24. Glatter O, Gruber K (1993) J Appl Cryst 26:512
25. Lippmaa E, Magi M, Samoson A, Tarmac M, Engelhardt G (1981) J Am Chem Soc 103:4992
26. Lippmaa E, Magi M, Samoson A, Engelhardt G, Grimmer AR (1980) J Am Chem Soc 102:4889
27. Ito T, Fraissard J (1982) J Chem Phys 76:5225
28. Fraissard J, Ito T (1988) Zeolites 8:350
29. Guzmán A, Lima E, Delahay G, Coq B, Lara V (2006) Ind Eng Chem Res 45:4163
30. Guzmán-Vargas A, Delahay G, Coq B (2003) Appl Catal B: Environ 42:369
31. Kieger S, Delahay G, Coq B, Neveu B (1999) J Catal 183:267
32. Chen HY, Voskoboinikov T, Sachtler WMH (1999) J Catal 186:91
33. Delahay G, Guzmán-Vargas A, Coq B (2007) Appl Catal B 70:45
34. Boulard S, Gilot P, Brosius R, Habermacher D, Martens JA (2004) Topics Catal 30–31:49